International Journal of Current Engineering and Technology
ISSN 2277 - 4106

Available at http://inpressco.com/category/ijcet

Research Article

Fault Analysis on Grid Connected MPPT based Photovoltaic System

Sibasish Panda[a*], Anup Kumar Panda[b] and H.N Pratihari[a]

[a]Dept- Electrical and electronics Engineering, Centurion University of technology & management, Paralakhemundi, Odisha, India
[b]Department of Electrical Engineering, NIT Rourkela, Rourkela, Odisha, India

Accepted 06 July 2013, Available online 01 August 2013, **Vol.3, No.3 (August 2013)**

Abstract

This paper presents the simulation model of a 3.5 kW PV array followed by a boost converter, which boost up the output voltage of the PV array. Maximum power point tracking (MPPT) can effectively improve the solar energy conversion efficiency of PV array, in this paper perturb- and – observe (P&O) algorithm has been used to achieve this function. Grid connected PV system needs a three phase inverter for synchronization. The inverter control system modeling has been carried out in Matlab/Simulink 2010 environment with the aids of the proportional-integral controllers, sinusoidal vectored pulse width modulation technique and park transformation. Phase locked loop (PLL) is used to lock the grid frequency and phase. Finally different types of AC faults are created on the grid side and total harmonic distortion (THD) is calculated in each of the case.

Keywords: *Photovoltaic (PV), Voltage source inverter (VSI), sinusoidal vectored pulse width modulation (SVPWM), Total harmonic distortion (THD), Maximum power point tracking (MPPT).*

1. Introduction

Renewable energy sources play an important role in electric power generation. Various renewable energy sources such as solar energy, wind energy, geothermal energy etc, are harness for electric power generation specifically solar energy has the advantages of no pollution, low maintenance cost, no installation area limitation and no noise due to the absence of moving parts. In recent years, photovoltaic (PV) systems have received unprecedented attention due to the concerns about adverse effects of extensive use of fossil fuels on the environment and energy security. Despite this high interest, grid connected PV systems are still outnumbered by the power generation schemes based on oil, natural gas, coal, nuclear, hydro, and wind (J. P. Benner *et al*, 1999). So far, PV system of capacities on the order of tens of megawatts have been installed and interfaced to the grid mainly at the primary distribution level.

The main drawbacks are the initial installation cost is considerably high and the energy conversion efficiency is relatively low, to overcome these problems the following two essential ways can be used (1) increase the efficiency of conversion of solar array (2) maximize the output power from the solar array. A grid-connected PV system includes a PV array, a voltage source inverter, an inverter control system, a load and a grid. The PV array consists of a number of individual photovoltaic cells that are connected in series and parallel array to convert sunlight to electricity by use of photovoltaic effect since the PV array produces DC power so the power electronics and control equipments are required to convert DC to AC power, this AC power is injected to utility grid.

Maximum power point tracking (MPPT) can effectively improve the solar energy conversion efficiency of PV system. In this paper *perturb- and – observe* (P&O) method is used to achieve this function. This paper establishes a dynamic model PV system by Matlab/simulink with d-axis and q-axis as coordinates which is synchronously rotating with the grid voltage to reflect the characteristics of system accurately. Reliability is an important issue in large-scale grid-connected photovoltaic (PV) systems as their operations rely on business plans developed over periods of time of at least twenty years, which often assume fault-free functioning. Not many papers discussing PV systems reliability are available in literature. For instance, (Stember LH *et al*, 1981) analyzes simple stand-alone PV systems using failure mode effect analysis (FMEA) and fault tree analysis (FTA). Failure rates estimates are also given assuming that time to failure is exponentially distributed. The failure rate for a PV array is hypothesized as being $33.3*10^{-6}$ failures/month, while inverter failure rate is assumed to be $342.5*10^{-6}$ failures/month (Hamdy MA *et al*, 2006). Since the inverter failure rate is more than the failure rate of PV array it is being necessary to analyze the fault in the inverter side i.e. L-G, L-L-G, L-L-L-G, L-L, L-L-L and the total harmonic distortion (THD)

*Corresponding author **Sibasish Panda** is working as Asst Professor, **Dr Anup Kumar Panda** and **Dr H.N Pratihari** as Professors.

is calculated for without fault condition and with different types of fault condition.

2. Mathematical Modeling

A. Modeling of PV cell

The direct conversion of the solar energy into electrical power is obtained by solar cells. A PV is composed by many strings of solar cells connected in series and in parallel combination, in order to provide desired values of output voltage and current.

The mathematical model of the PV cell is implemented in the form of a current source controlled by voltage, sensible to two input parameters, i.e. temperature (°C) and solar irradiation power (W/m^2). An equivalent simplified electric circuit of a photovoltaic cell is presented in Fig.1.

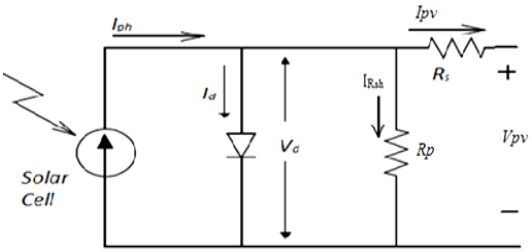

Fig.1. Equivalent circuit diagram of PV cell

The net current of the PV cell is the difference between the photo generated current I_{SC} and diode current I_d.

$$I_{PV} = I_{SC} - I_0*(e^{q*(V+I*R_S)/(n*K*T)}-1) \quad (1)$$

Where
I_0 is the reverse saturation current of the diode.
q is the electron charge (1.602*10^{-19} C).
V is the terminal voltage.
K is the Boltzmann constant (1.381*10^{-23} J/K)
T is the junction temperature in Kelvin (K)
Now equation (1) can be solved using Newton's method (Marcelo Gradella Villalva *et al*)
$x_{n+1} = x_n - f(x_n) / f'(x_n)$
Where: $f'(x)$ is the derivative of the function, $f(x) = 0$, x_n is a present value, and x_{n+1} is the next value.
Now equation (1) can be written as

$$f(I_{PV}) = I_{SC} - I - I_0*(e^{q*(V+I*R_S)/(n*K*T)}-1) = 0$$

Then using Newton's equation

$$I_{PV_{n+1}} = I_n - \frac{I_{SC} - I_n - I_0*(e^{q*(V+I_n*R_S)/(n*K*T)}-1)}{-1-(I_0*q*R_S*e^{[q*\frac{V+I_n*R_S}{n*K*T}]})/(n*K*T)} \quad (2)$$

The MATLAB function written to solve equation (2) performs the calculation five times iteratively.

The figure 2 and 3 represents the V-I and V-P characteristics of solar cell. The photon generated current at a given irradiance is given by(Marcelo Gradella Villalva; D. Sera *et al*,2007; W. De Soto *et al*, 2006)

$$I_{SC} = (I_{scn} + K_1 *\Delta T) * \frac{G}{G_n} \quad (3)$$

Where
I_{scn} = light-generated current at the nominal condition (Usually 25^{o}C and 1000W/m^2)
$\Delta T = T - T_n$ (T and T_n are the actual and nominal temperature in Kelvin)
G = Actual irradiance available.
G_n = Irradiance available under nominal condition.
The diode saturation current at a given temperature is given by (Q. Kou *et al*, 1998; R. A. Messenger, 2004; K.H. Hussein *et al*,1995)

$$I_0 = I_{0n} * (\frac{T}{T_n})^3 * e^{[(\frac{T}{T_n}-1)*\frac{E_g}{n*V_t}]} \quad (4)$$

Where
E_g = Bandgap energy of the semiconductor.
I_{0n} = Nominal reverse saturation current.
V_t = Junction thermal voltage It is a characteristic voltage that relates current flow in the p-n junction to the electrostatic potential across it.
Fig-4, 5, 6 and 7 represents the characteristics of solar cell under different irradiance and temperature.

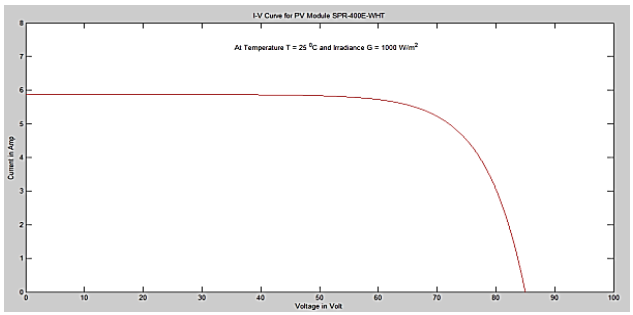

Fig.2. V-I characteristics of solar cell

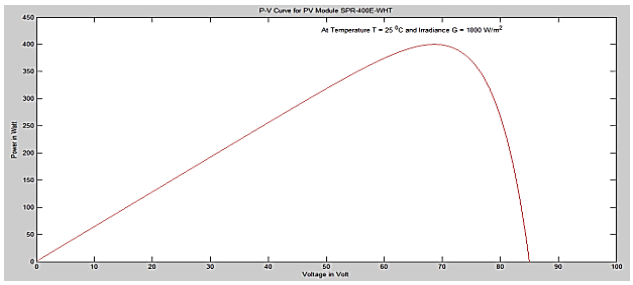

Fig.3. V-P characteristics of solar cell

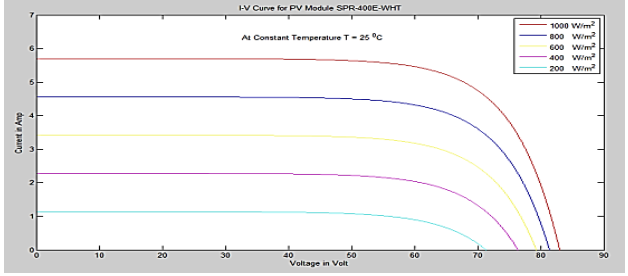

Fig.4. V-I characteristics of solar cell under constant temperature and different irradiance

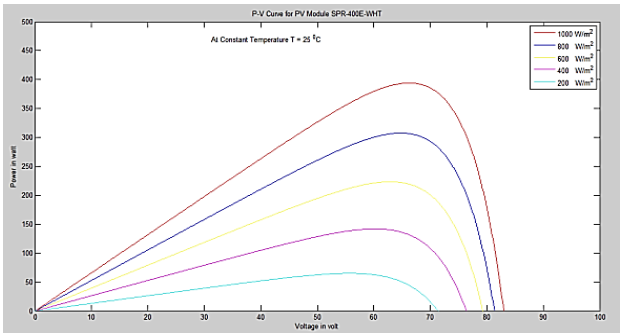

Fig.5. V-P characteristics of solar cell under constant temperature and different irradiance

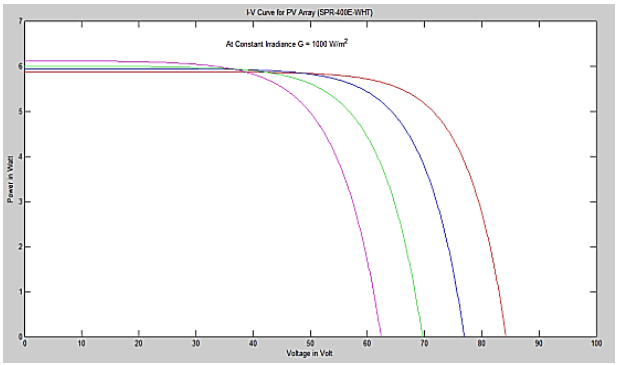

Fig.6. V-I characteristics of solar cell under constant irradiance and different temperature

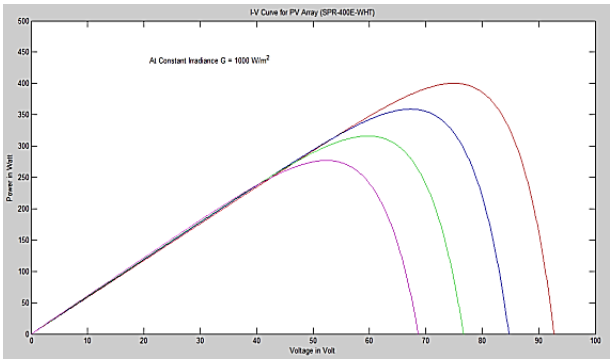

Fig.7. V-P characteristics of solar cell under constant irradiance and different temperature

B. Principle of MPPT algorithm

Peak power is reached with the help of a dc/dc converter between the PV generator and the load by adjusting its duty cycle such that the resistance matching is obtained. Now the question arises how to vary the duty cycle. The automatic tracking can be performed by implementing various algorithms. These algorithms are the heart of MPPT controller. The algorithm changes the duty cycle of the dc/dc converter to maximize the power output of the module and make it operate at the peak power point of the module. These techniques differ in many aspects such as required sensors, complexity, cost, range of effectiveness, convergence speed, correct tracking when irradiation and/or temperature change, hardware needed for the implementation or popularity, among others.

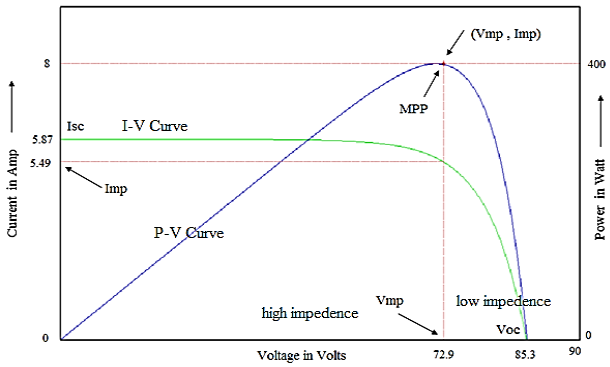

Fig.8. I-V & P-V curve & maximum power point

In this paper perturb and observe algorithm is implemented. In this algorithm a slight perturbation is introduced in to the system. Due to this perturbation the power of the module changes. If the power increases due to the perturbation then the perturbation is continued in that direction. After the peak power is reached the power at the next instant decreases and hence after that the perturbation reverses. At MPP, Vref = VMPP. Once the MPP is reached, operation of PV array is maintained at the point unless change in power is noted, indicating change in atmospheric conditions and the MPP. The algorithm decrements or increments Vref back to new MPP. The flowchart is shown in Fig.9.

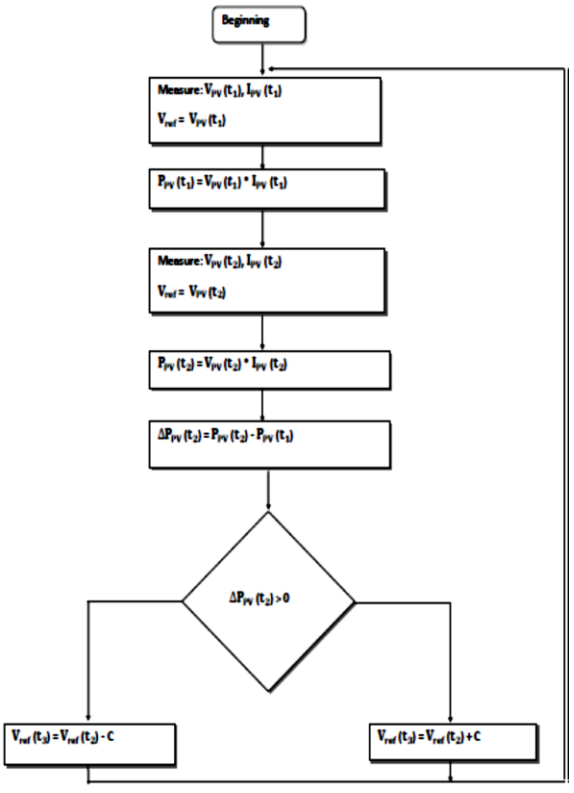

Fig.9. Flow Chart of perturb and observe algorithm

The above proposed algorithm can be designed by using Matlab/simulink, is given in Fig.10 and the output duty cycle is shown in Fig.11.

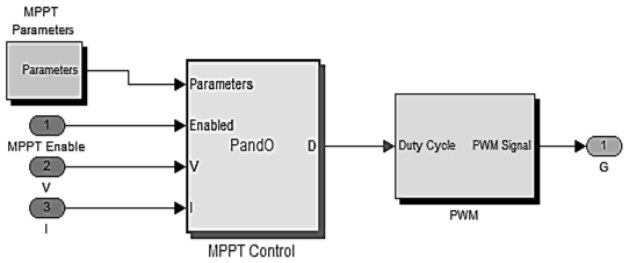

Fig.10. Matlab/Simulink model for the proposed MPPT algorithm

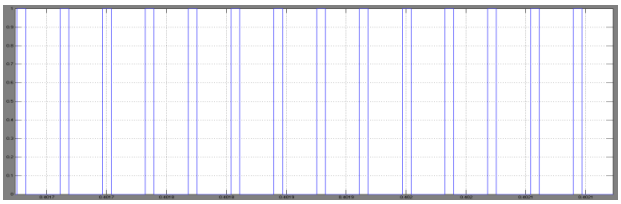

Fig.11. MPPT Output (Duty cycle)

3. Design details of the system

A. System Structure

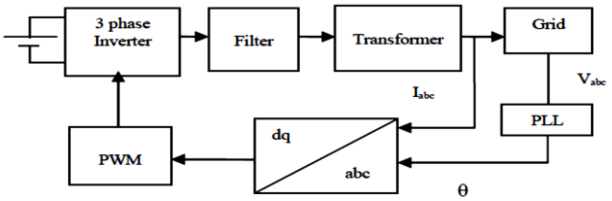

Fig.12. Block diagram of the system

A photovoltaic array of 3.5 kW is used to convert sunlight into DC current. The output of the array is connected to a boost DC converter that is used to perform MPPT functions and increase the array terminal voltage to a higher value so it can be interfaced to the distribution system grid of 25 kV. The DC converter controller is used to perform these two functions. A DC link capacitor is used after the DC converter and acts as a temporary power storage device to provide the voltage source inverter with a steady flow of power. The capacitor's voltage is regulated using a DC link controller that balances input and output powers of the capacitor. An LC low pass filter is connected at the output of the inverter to attenuate high frequency harmonics and prevent them from propagating into the power system grid. This provides a smooth output current which is low in harmonic content.

The voltage source inverter is controlled in the rotating *dq* frame to inject a controllable three phase AC current into the grid. To achieve unity power factor operation, current is injected in phase with the grid voltage. A phase locked loop (PLL) is used to lock on the grid frequency and provide a stable reference synchronization signal for the inverter control system, which works to minimize the error between the actual injected current and the reference current obtained from the DC link controller. The brief description of the controlling components of grid connected PV array system is discussed below.

B. LC Filter

Output voltage wave is synchronized with the grid voltage. So the PWM inverter will inject ripple current in to the grid. The output LC filter is connected to remove high switching frequency components from output current of inverter (Milan Pradanovic *et al*, 2003). The value of L is design based on current ripple. Smaller ripple results in lower switching and conduction losses. Typically the ripple current can be chosen as 10% - 15% of rated current. Considering 10% ripple at the rated current the designed value of inductor (L) in the system (C Y Wang *et al*,2003;Samul Araujo *et al*,2007)is given by (5)

$$\Delta i_{Lmax} = \frac{1}{8} * V_{dc} / \mathrm{L} * f_s \quad (5)$$

The capacitor C is designed based on reactive power supplied by the capacitor at fundamental frequency. In this design reactive power is chosen as 15% of the rated power (C Y Wang *et al*, 2003) is given by (6)

$$\mathrm{C} = 15\% * P_{rated} / 3 * 2\pi \mathrm{f} * V_{rated}^2 \quad (6)$$

C. Phase Locked Loop

Grid synchronizations plays important role for grid connected systems. It synchronizes the output frequency and phase of grid voltage with grid current using different transformation. Different methods to extract phase angle have been developed and presented in many papers (S.K. Chung *et al*,2000; Guan Chyan Hsieh *et al*,1999). PLL techniques causes one signal to track another one. Phase-locked loop (PLL) is a feedback loop which locks two waveforms with same frequency but shifted in phase. The fundamental use of this loop is in comparing frequencies of two waveforms and then adjusting the frequency of the waveform in the loop to equal the input waveform frequency. The role of the phase locked loop is to provide the rotation frequency, direct and quadrature voltage components at the point of common coupling (PCC) by resolving the grid voltage *abc* components. Multiple control blocks of the PV system rely on this information to regulate their output command signals. The PLL computes the rotation frequency of the grid voltage vector by first transforming it to the *dq* frame, and then force the quadrature component of the voltage to zero to eliminate cross coupling in the active and reactive power terms (Xiao-Qiang Guo *et al*.

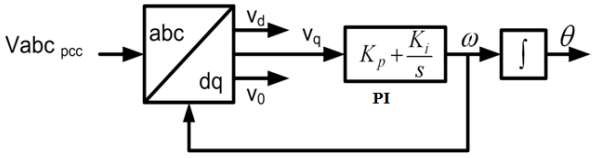

Fig.13. Schematic diagram of the phase locked loop (PLL)

The loop filter PI is a low pass filter. It is used to suppress high frequency component and provide DC controlled signal to voltage controlled oscillator (VCO) which acts as an integrator. The output of the PI controller is the inverter output frequency that is integrated to obtain inverter phase angle θ. When the difference between grid phase angle and inverter phase angle is reduced to zero PLL becomes active which results in synchronously rotating voltages Vd = 0 and Vq gives magnitude of grid voltage. The operation of the PLL is governed by equation (7)

$$\left.\begin{aligned}\omega &= K_p V_q + K_i \int V_q dt \\ \theta &= \int \omega \, dt\end{aligned}\right\} \quad (7)$$

D. Space Vector PWM

The space vector PWM (SVM) method is an advanced, computation-intensive PWM method and is possibly the best method among the all PWM techniques. The circuit model of a typical three-phase voltage source PWM inverter is shown in Fig.14.

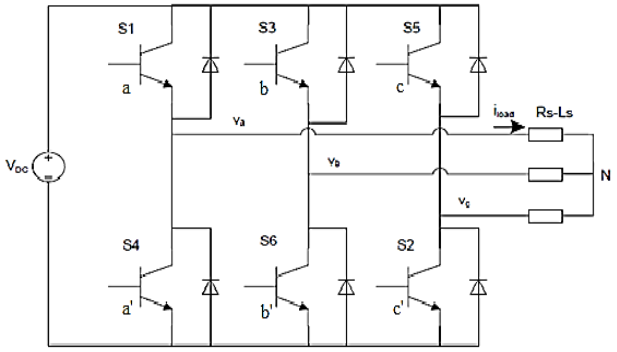

Fig.14. Three-phase inverter

S1 to S6 are the six power switches that shape the output, which are controlled by the switching variables $a,\ a',\ b,\ b',\ c\ and\ c'$. When an upper transistor is switched on, i.e., when a, b or c is 1, the corresponding lower transistor is switched off, i.e., the corresponding a′, b′ or c′ is 0. Therefore, the on and off states of the upper transistors S1, S3 and S5 can be used to determines the output voltage.

The relationship between the switching variable vector $[a \quad b \quad c]^t$ and the line-to-line voltage vector $[V_{ab} \quad V_{bc} \quad V_{ca}]^t$ is given by equation (8) in the following:

$$\begin{bmatrix} V_{ab} \\ V_{bc} \\ V_{ca} \end{bmatrix} = V_{dc} \begin{bmatrix} 1 & -1 & 0 \\ 0 & 1 & -1 \\ -1 & 0 & 1 \end{bmatrix} \begin{bmatrix} a \\ b \\ c \end{bmatrix} \quad (8)$$

Also, the relationship between the switching variable vector $[a \quad b \quad c]^t$ and the phase voltage vector $[V_a \quad V_b \quad V_c]^t$ can be expressed by equation 9

$$\begin{bmatrix} V_{an} \\ V_{bn} \\ V_{cn} \end{bmatrix} = \frac{V_{dc}}{3} \begin{bmatrix} 2 & -1 & -1 \\ -1 & 2 & -1 \\ -1 & -1 & 2 \end{bmatrix} \begin{bmatrix} a \\ b \\ c \end{bmatrix} \quad (9)$$

There are eight possible combinations of on and off patterns for the three upper power switches (P.Tripura *et al*, 2011. The on and off states of the lower power devices are opposite to the upper one and so are easily determined once the states of the upper power transistors are determined. The eight switching vectors, output line to neutral voltage (phase voltage), and output line-to-line voltages in terms of DC-link Vdc, are given in Table 1 and Fig.15 shows the eight inverter voltage vectors (V0 to V7).

Table 1: Switching vectors, phase voltages and output line to line voltages.

Voltage Vectors	Switching Vectors			Line to neutral voltage			Line to line voltage		
	a	b	c	V_{an}	V_{bn}	V_{cn}	V_{ab}	V_{bc}	V_{ca}
V_0	0	0	0	0	0	0	0	0	0
V_1	1	0	0	2/3	-1/3	-1/3	1	0	-1
V_2	1	1	0	1/3	1/3	-2/3	0	1	-1
V_3	0	1	0	-1/3	2/3	-1/3	-1	1	0
V_4	0	1	1	-2/3	1/3	1/3	-1	0	1
V_5	0	0	1	-1/3	-1/3	2/3	0	-1	1
V_6	1	0	1	1/3	-2/3	1/3	1	-1	0
V_7	1	1	1	0	0	0	0	0	0

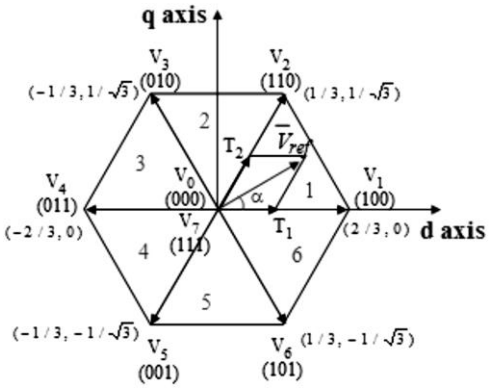

Fig.15. Basic switching vectors and sectors

To implement the space vector PWM, the voltage equations in the *abc* reference frame can be transformed into the stationary *dq* reference frame that consists of the horizontal (d) and vertical (q) axes as depicted in Fig.16. The eight vectors are called the basic space vectors and are denoted by V0, V1, V2, V3, V4, V5, V6, and V7. Therefore, space vector PWM can be implemented by the following steps

Step 1. Determine *Vd, Vq, Vref,* and angle (α)

Step 2. Determine time duration T1, T2, T0

Step 3. Determine the switching time of each transistor (S1 to S6)

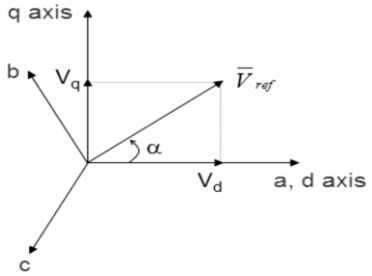

Fig.16. Voltage Space Vector and its components in (d, q)

$$\begin{bmatrix} V_d \\ V_q \end{bmatrix} = \frac{2}{3}\begin{bmatrix} 1 & -\frac{1}{2} & -\frac{1}{2} \\ 0 & \frac{\sqrt{3}}{2} & -\frac{\sqrt{3}}{2} \end{bmatrix}\begin{bmatrix} V_{an} \\ V_{bn} \\ V_{cn} \end{bmatrix} \quad (10)$$

$$|\bar{V}_{ref}| = \sqrt{V_d^2 + V_q^2} \quad (11)$$

$$\alpha = \tan^{-1}\frac{V_q}{V_d} = \omega t = 2\pi f t \quad (12)$$

where f = fundamental frequency

4. MATLAB SIMULINK model and fault analysis

A. Simulink Model

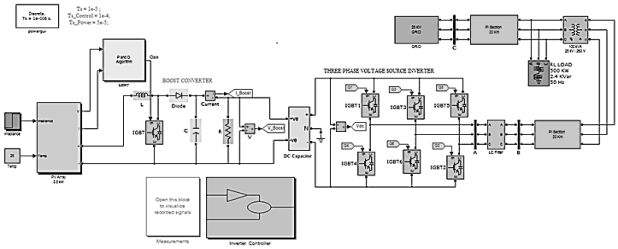

Fig.17. Simulink Model of Grid Connected PV System

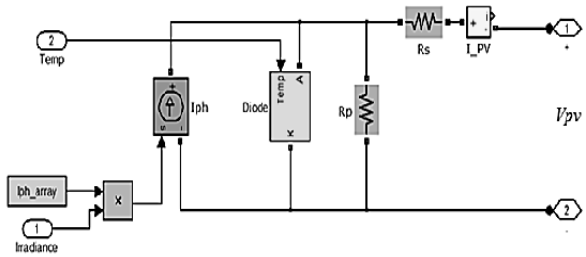

Fig.18. Equivalent PV cell model in Simulink

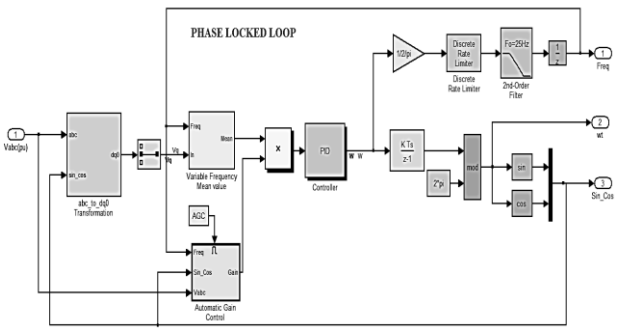

Fig.19. Simulink model of Phase Locked Loop (PLL)

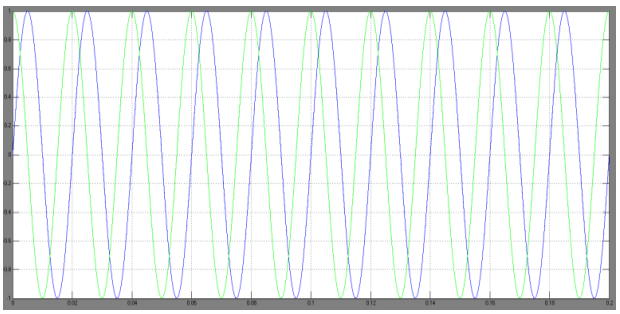

Fig.20. sin and cos wave generated by PLL

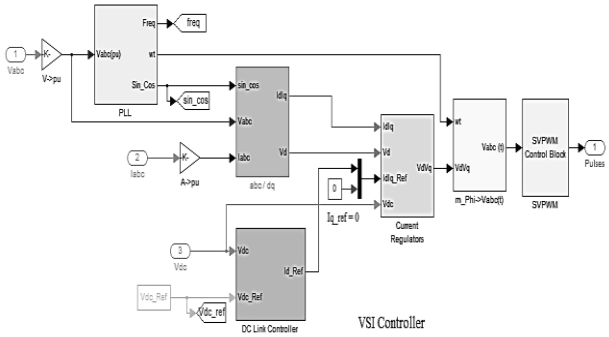

Fig.21. Simulink model of VSI controller

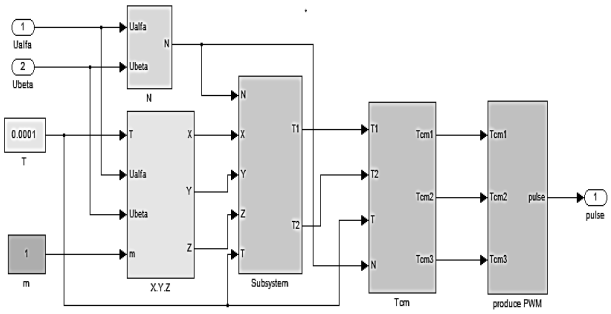

Fig.22. Simulink model of Space Vector PWM

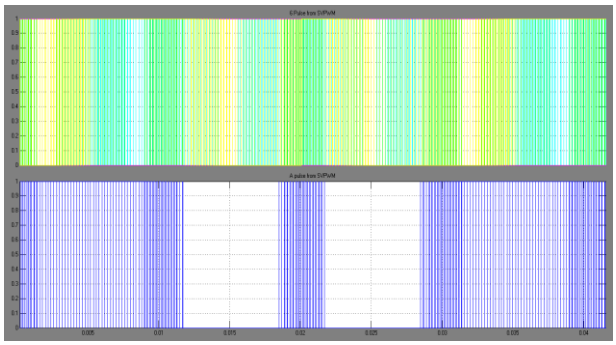

Fig.23. Output of SVPWM

To simulate the system and the resulting output currents and voltages at various levels, the array was subjected to a 1000 W/m^2 of solar irradiation and a temperature of 25° C. The DC output current, terminal voltage and power of PV array was monitored during simulation at the specified atmospheric conditions. The switching action of the DC converter caused some ripple in the output current with an average value of about 13.5 A, the ripple magnitude can be reduced by increasing the size of the inductor used in the boost converter. There are some initial transients in the current waveform at the beginning of simulation as the system started operation and the DC converter drove the array to the estimated maximum power point. All the simulations given below are for 0.5 seconds. Fig.24, 25 shows the comparison of voltage, current and power of PV array without and with MPPT and boost converter power with MPPT respectively. It can be observed that PV array feeds 3.5 kW to the inverter using MPPT. Without MPPT the power reduces drastically from 3.5 kW to 2.9 kW.

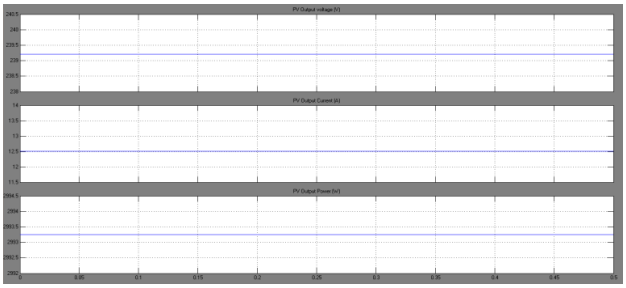

Fig.24. Voltage, Current and Power Output of PV array without MPPT

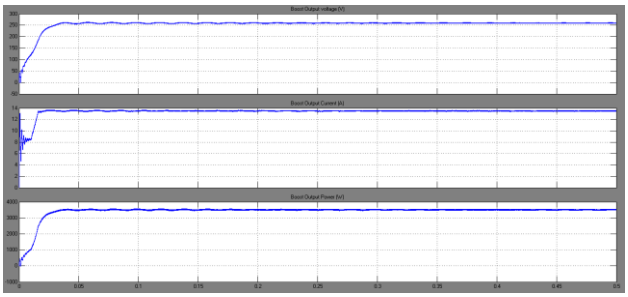

Fig.25. Voltage, Current and Power Output of PV array with MPPT

B. Fault Analysis

The grid connected PV array system in Simulink is shown in Fig.17. The system is studied under different fault conditions which are shown below. The system is simulated at irradiance G = 1000 W/m^2 and temperature T=25 ^{0}C. The fault is given only on the grid side. The fault duration is for 0.1 seconds from 0.2 to 0.3 seconds. The waveforms of grid side as well as inverter side are shown. Also voltage and current magnitudes and active and reactive power are also presented which varies with different fault conditions. First the system is simulated without fault.

1. Without Fault

The inverter output for 260 V dc input is shown in Fig.25. As seen in Fig.27, 28, and 29 there is no transients in any of the waveforms. Even there is no deviation in the active and reactive power curve while the reactive power being slightly greater than zero.

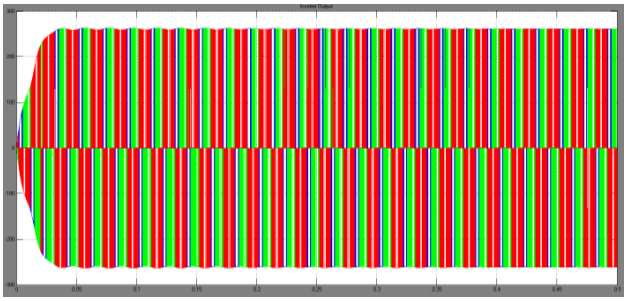

Fig.26. Voltage waveform before filter

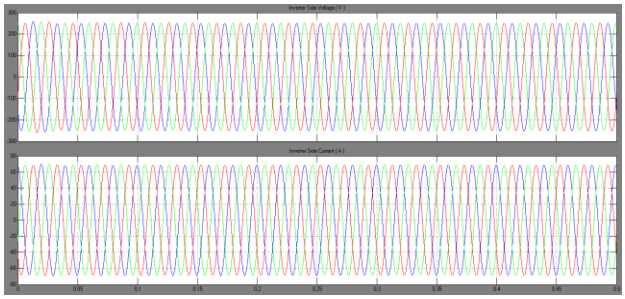

Fig.27. Voltage and Current waveforms on the inverter side

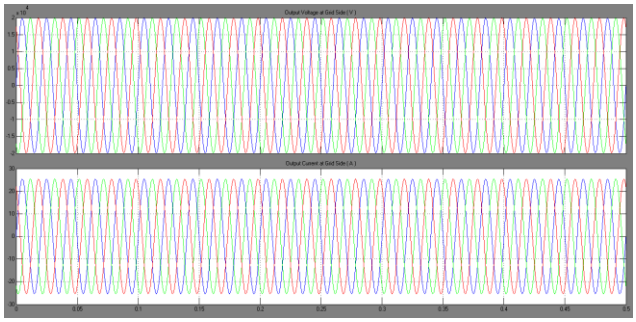

Fig.28 Voltage and Current waveforms on the Grid side

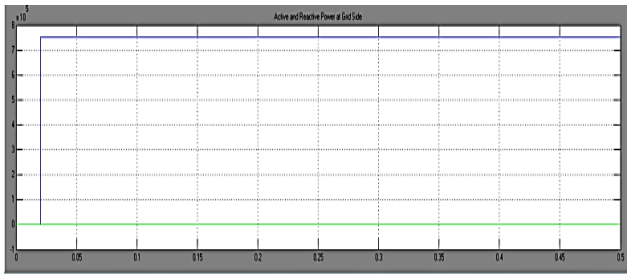

Fig.29. Active and Reactive Power of Grid

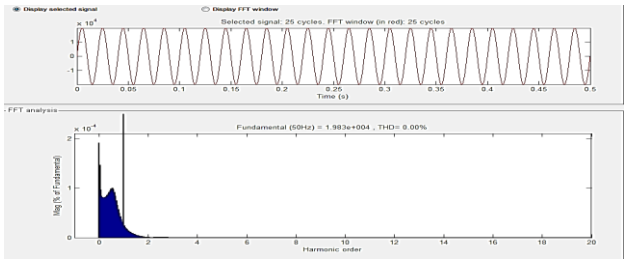

Fig.30. Grid side FFT and THD for Voltage

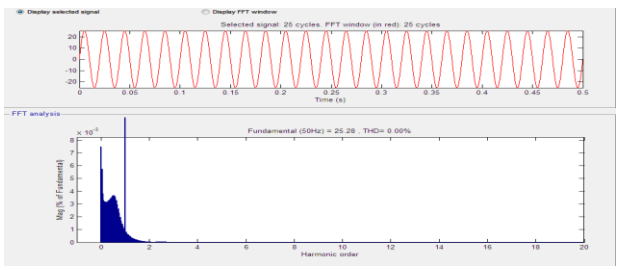

Fig.31. Grid side FFT and THD for Current

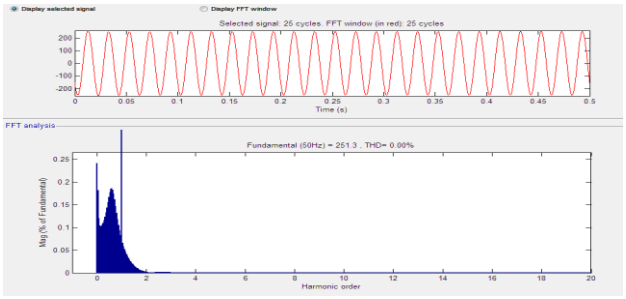

Fig.32. Inverter side FFT and THD for Voltage with filter

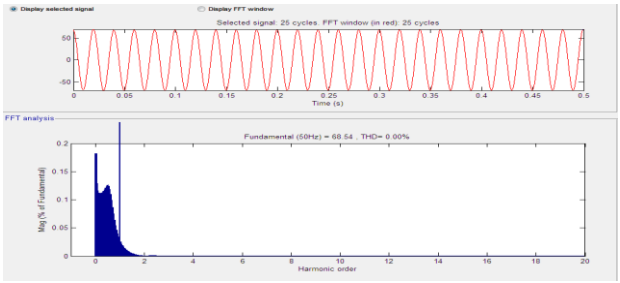

Fig.33. Inverter side FFT and THD for Voltage with filter

2. LG Fault

In line to ground fault, a phase of voltage waveforms collapse as seen in Fig.34 and the magnitude of current of a phase increases to 850 A. Also the active and the reactive power in Fig.35 deviate from their nominal values. The reactive power which remains nearly zero during no fault increases to 3.5 MVAR while the active power rises up to 6.2 MVA. In this case THD of voltage is increased from 0% to 0.04% in inverter side and 0.44% in grid side. The THD of current is also increased from 0% to 0.07% in inverter side and 1.08% in grid side.

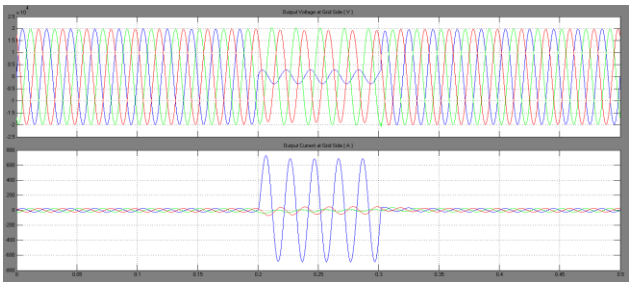

Fig.34. Voltage and Current waveforms on the grid side with LG fault

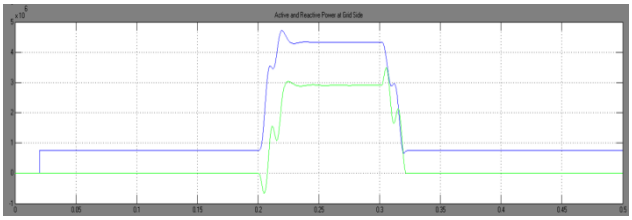

Fig.35. Active and Reactive Power of Grid during LG fault

3. LL Fault

In line to line fault two phases of voltage waveforms collapse and two phases of current waveforms shoots to high magnitude as shown in Fig.36. During fault the active power rises from 0.9 MVA to 6.1 MVA whereas reactive power rises from 0 to 4 MVAR. In this case THD of voltage is increased from 0% to 0.22% in inverter side and 1.04% in grid side. The THD of current is also increased from 0% to 0.23% in inverter side and 3.45% in grid side.

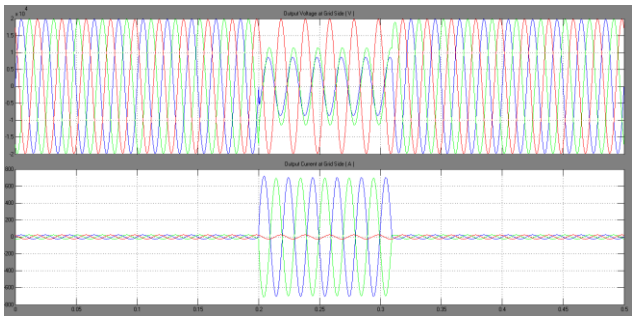

Fig.36. Voltage and Current waveforms on the grid side with LL fault

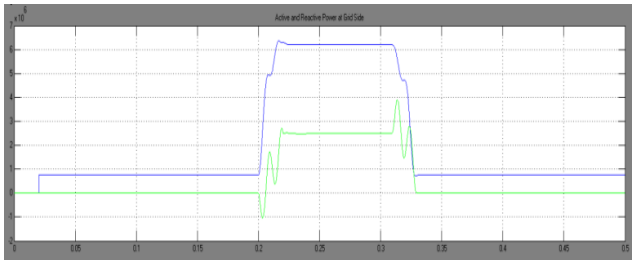

Fig.37. Active and Reactive Power of Grid during LL fault

4. LLG Fault

Comparing LL and LLG faults, the fault current is higher in LLG fault as shown in Fig.38. But, during fault, the active power is lower and reactive power is higher in LLG fault than LL fault. In this case THD of voltage is increased from 0% to 0.12% in inverter side and 0.41% in grid side. The THD of current is also increased from 0% to 0.06% in inverter side and 1.09% in grid side.

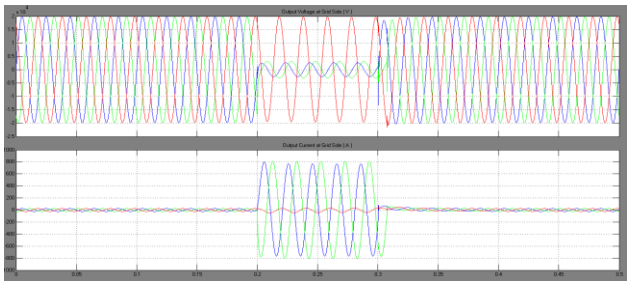

Fig.38. Voltage and Current waveforms on the grid side with LLG fault

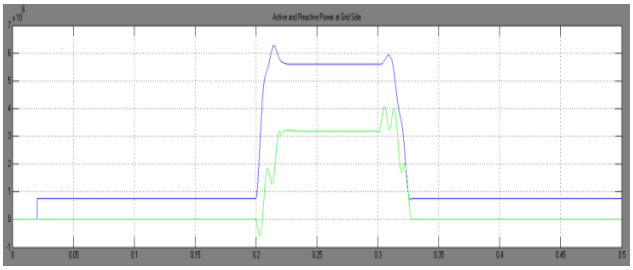

Fig.39. Active and Reactive Power of Grid during LLG fault

5. LLL Fault

In symmetric three phase fault, all the three phases of voltage waveforms collapse and the current magnitude becomes very high during fault shown in Fig.40. The pattern of active and reactive power during three phase fault is presented in Fig.41. In this case THD of voltage is increased from 0% to 0.04% in inverter side and 0.23% in grid side. The THD of current is also increased from 0% to 0.23% in inverter side and 0.71% in grid side.

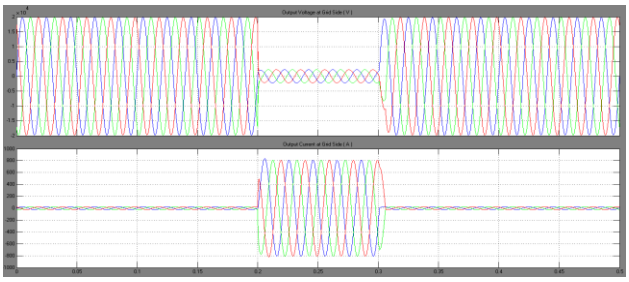

Fig.39. Voltage and Current waveforms on the grid side with LLL fault

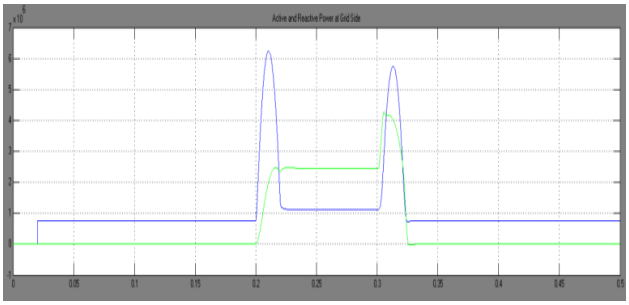

Fig.40. Active and Reactive Power of Grid during LLL fault

6. LLLG Fault

The waveforms of three phase to ground fault is similar to three phase fault except there is slight increase in fault current in LLLG shown in Fig.42. As LLLG fault is severe than any other fault, it can be concluded that fault on the grid side will hardly effects on the PV and boost converter side with other type of faults on ac side. In this case THD of voltage is increased from 0% to 0.04% in inverter side and 0.23% in grid side. The THD of current is also increased from 0% to 0.23% in inverter side and 0.71% in grid side.

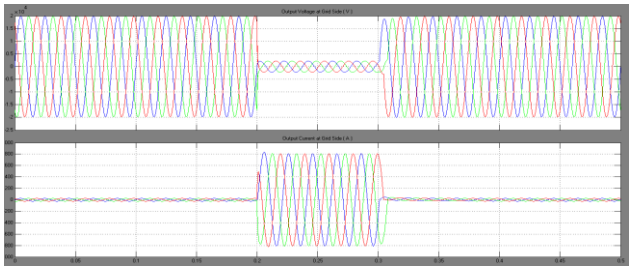

Fig.41. Voltage and Current waveforms on the grid side with LLLG fault

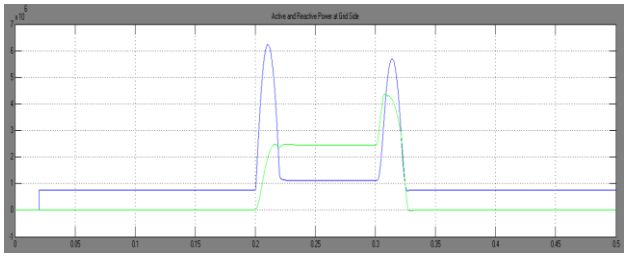

Fig.42. Active and Reactive Power of Grid during LLLG fault

Fig.43 represents the frequency (in Hz) for synchronisation taken from PLL. The system was simulated for 1.0 second to have a clear examination on the locking process. It is found that for synchronisation between PV system and grid, it is taking 0.15 second. When LLLG fault is created between 0.4 to 0.5 s, the frequency deviates from its nominal frequency of 50 Hz. It takes another 0.2 s (0.5 to 0.7s) for the system to become stable at nominal frequency. Even though the operating frequency deviates from its nominal value, it remains within the limits of 49 Hz – 51 Hz. (in this case its between 49.7 and 50.6 Hz).

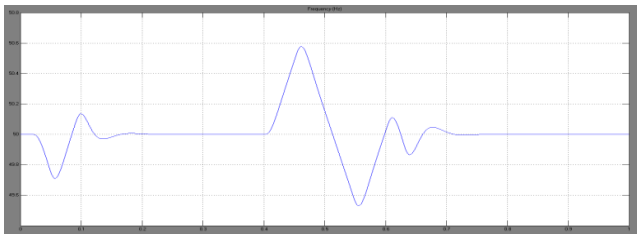

Fig.43. System frequency (Hz)

5. Conclusion

A 3.5 kW PV array with MPPT has been modeled and simulated. The MPPT employed perturb and observe algorithm. The simulated results confirm the effectiveness of the MPPT. It is observed that with MPPT the power fed to the inverter from PV array has increased by 14%. A PLL has been designed for grid synchronization and it effectively synchronizes the inverter voltage and

frequency with the grid voltage and frequency. In case of fault it is observed that it takes only 0.2 sec for the system to become stable at nominal frequency. Fault analysis on grid side have been performed for various fault conditions like; LG, LL, LLL, LLG faults. The variations of active and reactive power and variation of voltage and current THD without fault and with fault conditions are studied. The findings of the fault analysis are essential for designing the protection circuit.

Appendix

Table .2 Module parameters of SPR 400E-WHT

PV Parameter	*Specifications*	*Comments*
V_{oc}	85.2983V	Open circuit voltage
I_{sc}	5.8675A	Short circuit current
V_{mp}	72.8992V	Voltage at maximum power
I_{mp}	5.48769A	Current at maximum power
P_{mp}	400 W	Maximum power
I_{sc} temperature coefficient	0.001837 A/°C	Short circuit current temperature coefficient

Table .3 System Specifications

Parameter	*Specifications*	*Comments*
V_{oc}	255.895V	Array Open circuit voltage
I_{sc}	17.60A	Array Short circuit current
V_{mp}	218.697V	Array Voltage at maximum power
I_{mp}	16.461A	Array Current at maximum power
P_{mp}	3600W	Array Maximum power
System frequency	50Hz	
Grid Voltage	25kV	Line to Line
Inverter voltage	260V	Line to Line
Grid inductance	3mH	
Grid resistance	20Ω	
Switching frequency	4000Hz	
Inductive Load	500kW	Real Power
	2.4kVAR	Reactive Power
Interfacing transformer	260V	Primary Side
	25kV	Secondary Side

Table.4 THD of voltage and current for different types of AC faults

Parameters	Type of Fault	Inverter side THD (Phase A) in %	Grid side THD (Phase A) in %
Voltage	Without Fault	0.0	0.0
	LG	0.04	0.44
	LLG	0.12	0.41
	LL	0.22	1.04
	LLL	0.04	0.23
	LLLG	0.10	0.22
Current	Without Fault	0.0	0.0
	LG	0.07	1.08
	LLG	0.06	1.09
	LL	0.23	3.65
	LLL	0.23	0.71
	LLLG	0.20	0.67

References

J. P. Benner and L. Kazmerski (Sep. 1999), "Photovoltaics gaining greater visibility," *IEEE Spectr.*, vol. 36, no. 9, pp. 34–42,

Stember LH (1981) Reliability considerations in the design of solar photovoltaic power systems. *Solar Cells3*(3):269e85.

Hamdy MA, Beshir ME, Elmasry SE (1989),Reliability analysis of photovoltaics systems. *Applied Energy* 33(4):253e63.

David M. Bressoud (June 20, 2006), Radical Approach to Real Analysis 2nd edition 2006

Jonas Rafael Gazoli,Modeling And Circuit-Based Simulation of Photovoltaic Arrays Marcelo *Gradella Villalva, Ernesto Ruppert FilhoUniversity of Campinas* (UNICAMP), Brazil.

D. Sera, R. Teodorescu, and P. Rodriguez (2007), PV panel model based on datasheet values. In *Proc. IEEE International Symposium on Industrial Electronics, ISIE*, p. 2392–2396.

W. De Soto, S. A. Klein, and W. A. Beckman(Jan 2006), Improvement and validation of a model for photovoltaic array performance. *Solar Energy*, 80(1):78–88.

A. Driesse, S. Harrison, and P. Jain (2007), Evaluating the effectiveness of maximum power point tracking methods in photovoltaic power systems using array performance models. In *Proc. IEEE Power Electronics Specialists Conference, PESC*, p. 145–151.

Q. Kou, S. A. Klein, and W. A. Beckman (Sept 1998), A method for estimating the long-term performance of direct-coupled PV pumping systems. *Solar Energy*, 64(1-3):33–40.

R. A. Messenger and J. Ventre (2004), Photovoltaic systems engineering. *CRC Press*.

K.H. Hussein, I. Muta, T. Hoshino, and M. Osakada(Jan 1995), Maximum photovoltaic power tracking: an algorithm for rapidly changing atmospheric conditions. *In Generation, Transmission and Distribution, IEEE Proceedings*-, v. 142, p. 59–64.

Milan Pradanovic & Timothy Green (Jan 2003), Control and filter design of three phase inverter for high power quality grid connection, *IEEE transactions on Power Electronics*,Vol.18. pp.1- 8.

C Y Wang,Zhinhong Ye& G.Sinha (2003), Output filter design for a grid connected three phase inverter, *Power electronics Specialist Conference*, pp.779-784,PESE.

Samul Araujo& Fernando Luiz (Oct 2007), LCL fiter design for grid connected NPC inveters in offshore wind turbins,*7th*

International conference on Power Electronics, pp. 1133-1138.

S.K. Chung (May 2009), Phase lock loop for grid connected 3 phase power conversion system, *IEE Proc. Electr. Power Application*, Vol. 147, pp. 213 – 219.

Guan Chyan Hsieh & James .C Hung (Dec 1999), Phase- Lock Loop Techniques - A Survey ,*IEEE Transaction on Industrial Electronics*, Vol. 43, pp. 50- 60, December.

Xiao-Qiang GUO, Wei-Yang WU, He-Rong GU (2011), "Phase locked loop and synchronization methods for grid-interfaced converters: a review", *Przeglad Elektrotechniczny (Electrical Review)*

P.Tripura, Y.S.Kishore Babu, Y.R.Tagore (Oct 2011), "Space Vector Pulse Width Modulation Schemes for Two-Level Voltage Source Inverter", ACEEE Int. J. on Control System and Instrumentation Vol. 02, No. 03.